Nanoscale Research Letters

NANO EXPRESS Open Access

# High-Performance Deep Ultraviolet Photodetector Based on NiO/β-$Ga_2O_3$ Heterojunction

Menghan Jia[1,2,3], Fang Wang[1,2,3], Libin Tang[2,3*], Jinzhong Xiang[4*], Kar Seng Teng[5*] and Shu Ping Lau[6]

## Abstract

Ultraviolet (UV) photodetector has attracted extensive interests due to its wide-ranging applications from defense technology to optical communications. The use of wide bandgap metal oxide semiconductor materials is of great interest in the development of UV photodetector due to their unique electronic and optical properties. In this work, deep UV photodetector based on NiO/β-$Ga_2O_3$ heterojunction was developed and investigated. The β-$Ga_2O_3$ layer was prepared by magnetron sputtering and exhibited selective orientation along the family of ($\bar{2}$ 01) crystal plane after annealing. The photodetector demonstrated good performance with a high responsivity ($R$) of 27.43 $AW^{-1}$ under a 245-nm illumination (27 $\mu Wcm^{-2}$) and the maximum detectivity ($D^*$) of $3.14 \times 10^{12}$ $cmHz^{1/2}\,W^{-1}$, which was attributed to the p-NiO/n-β-$Ga_2O_3$ heterojunction.

**Keywords:** β-$Ga_2O_3$, NiO, Heterojunction, UV photodetector

## Background

There have been much research interests in the development of ultraviolet (UV) photodetectors due to their wide-ranging applications, such as missile warning, biochemical analysis, flame and ozone detections, and optical communications. As compared to SiC and GaN semiconductors, UV photodetectors based on wide bandgap metal oxide semiconductors offer many advantages. For example, the metal oxide-based photodetectors do not oxidize easily and exhibit sensitive response. Furthermore, they are easy to operate and can be made small in size [1, 2]. Hence, wide bandgap metal oxides and their devices have attracted much research attention in recent years. To date, metal oxides such as ZnO [3–5], $TiO_2$ [6, 7], $SnO_2$ [8], NiO [9], and $Ga_2O_3$ [10, 11] have been studied for use as high-performance UV photodetectors. Among them, the stable phase of $Ga_2O_3$ (β-$Ga_2O_3$) is becoming a preferred material for UV photodetector as it is a direct bandgap semiconductor with ultra-wide bandgap of ~ 4.9 eV that responses to the UV band effectively. The facile growth process of the material is an added advantage.

Several groups have attempted to enhance the performance of UV photodetectors by developing heterojunction devices consisting of two different metal oxide semiconductors. For example, Zhao et al. reported the studies of ZnO-$Ga_2O_3$ core-shell heterostructure UV photodetectors, which demonstrated ultra-high responsivity and detectivity due to an avalanche multiplier effect [12, 13]. In this work, a different metal oxide heterojunction, such as NiO/β-$Ga_2O_3$, was investigated to provide a high-performance UV photodetector. Firstly, the lattice mismatch of β-$Ga_2O_3$ and NiO is relatively small. Also, the bandgap of NiO is larger than that of ZnO used in previous study. The p-type behavior of NiO and n-type β-$Ga_2O_3$ has led to several reports on the studies of the electrical properties of NiO/β-$Ga_2O_3$ heterojunction for power electronics applications [14]; however, there is limited report on the use of the heterojunction in photodetector. In this study, the NiO/β-$Ga_2O_3$-based UV photodetector was produced by magnetron sputtering on indium tin oxide (ITO) transparent substrate. The results showed that the NiO/β-$Ga_2O_3$ photodetector exhibited excellent sensitivity to UV light (245 nm) with good stability.

* Correspondence: scitang@163.com; jzhxiang@ynu.edu.cn; k.s.teng@swansea.ac.uk
[2]Kunming Institute of Physics, Kunming 650223, China
[4]School of Physics and Astronomy, Yunnan University, Kunming 650091, China
[5]College of Engineering, Swansea University, Bay Campus, Fabian Way, Swansea SA1 8EN, UK
Full list of author information is available at the end of the article

## Methods

$Ga_2O_3$ and NiO ceramic targets (99.99%) were purchased from Zhongnuo Advanced Material (Beijing) Technology Co. Ltd. Sapphire substrate with (0001) plane was purchased from Beijing Physike Technology Co. Ltd. ITO-coated quartz substrate was purchased from Beijing Jinji Aomeng Technology Co. Ltd. All chemical reagents used in the experiments were used without further purification.

β-$Ga_2O_3$ film was prepared by RF magnetron sputtering at room temperature. For characterization, the film was deposited on to sapphire substrate with (0001) plane. Prior to deposition, the substrate was wet-cleaned in a mixed solution of ammonia water, hydrogen peroxide, and deionized water (1:1:3) at 80 °C for 30 min. It was rinsed repeatedly with deionized water and dried using nitrogen to remove surface fouling, which would enhance uniformity and adhesion of the film on the substrate. Sputtering was performed at a pressure of 0.7 Pa with oxygen and argon flowing at a rate of 5 and 95 sccm, respectively. A sputtering power of 200 W was used for a duration of 60 min in the deposition of the film. Finally, the deposited film was annealed in air at 800 °C (60 min) at a heating rate of 10 °C/min.

Crystalline structure of the $Ga_2O_3$ film was studied using X-ray diffraction (XRD, EMPYREAN) and transmission electron microscope (TEM, JEM-2100). Absorption spectra of the $Ga_2O_3$ film on sapphire substrate were measured by UV-Vis spectroscopy (iHR-320), which also provided an estimation on optical bandgap of the film. The surface morphology and thickness of the deposited $Ga_2O_3$ film were characterized using atomic force microscope (AFM, SPA-400) and optical microscope (LEICA DM 2700 M). Elemental analysis of the $Ga_2O_3$ film was performed by X-ray photoelectron spectroscopy (XPS, K-Alpha+). Current-voltage (*J-V*) measurement on the NiO/β-$Ga_2O_3$ photodetector was carried out with a Keithley 2400 source meter. All measurements were conducted at room temperature.

## Results and Discussion

Figure 1a show the XRD patterns of the $Ga_2O_3$ film grown on (0001) plane of sapphire substrate before and after annealing. Before annealing, the as-deposited film exhibited an amorphous state as only two peaks (marked as "*") that associated with the substrate were observed in the pattern. After annealing the film at 800 °C, the XRD pattern showed six characteristic peaks corresponding to crystal planes of β phase of $Ga_2O_3$, which belongs to the monoclinic crystal system. The observed pattern is consistent with previously reported work [15, 16]. These characteristic peaks of the annealed β-$Ga_2O_3$ film revealed good crystallinity with preferential orientation along the family of $(\bar{2}\,01)$ crystal planes.

Figure 1d and e are TEM and HRTEM images of the β-$Ga_2O_3$ film after annealing. As shown, the lattice fringe spacing of $(\bar{2}\,01)$, (400), and $(\bar{2}\,02)$ crystal planes were 4.69 Å, 2.97 Å, and 2.83 Å, respectively, which again suggests good crystallinity and is in good agreement with previously reported work in the literature [17, 18].

AFM image of the β-$Ga_2O_3$ film deposited on sapphire substrate is shown in Fig. 1f. The as-deposited film exhibited a uniform granular surface topography with relatively small root-mean-square (RMS) surface roughness of 1.36 nm. After annealing, the RMS roughness of the film increased to 1.68 nm. Such increase in the RMS roughness after annealing was also reported by Hao et al [19]. It is possible that the annealing treatment could result in surface structural defects. Further studies are required to understand the cause of change in surface morphology after annealing. AFM topography images of the step edge between the film and substrate before and after annealing are shown in Fig. 1 g and h, which the line profiles (in the inset) indicated a film thickness of 114 ± 6.4 nm and 123 ± 2.0 nm (about 8% increase), respectively. The increase in film thickness and RMS after annealing could be that the phase transition from amorphous to crystallinity leads to the nanocrystal grain growth.

UV-Vis absorption spectra of the β-$Ga_2O_3$ films before and after annealing are shown in Fig. 1b. Both films exhibited strong UV absorption in the range of 190–300 nm and almost no absorption in the visible light band. This showed that the annealing treatment did not have a significant effect on the absorption edge. It only resulted in a small red shift of about 10 nm with slight enhancement on the absorption peak. Eq. (1) can be used to estimate the optical bandgap energy (*Eg*) of the film.

$$\alpha(h\nu) = A(h\nu - Eg)^{1/2} \tag{1}$$

where $\alpha$ is absorption coefficient, $h\nu$ is photon energy, and $A$ is a constant. Taking into account of the film thicknesses measured by AFM, the *Eg* of the as-deposited and annealed films can be determined from the plots in Fig. 1c, which indicated a value of 5.137 eV and 5.135 eV, respectively. These values are close to the theoretical *Eg* of 4.9 eV for β-$Ga_2O_3$.

XPS spectra of the β-$Ga_2O_3$ film are shown in Fig. 2. Figure 2a–c and d–f show XPS spectra of the full scan, Ga and O elements before and after annealing, respectively. The C element observed from the full scan was adventitious carbon. After annealing, the C 1 s peak was reduced significantly indicating that most carbon was removed during the annealing treatment. The binding energy of Ga3d in Fig. 2 b and e correspond to 21.14 eV and 20.70 eV, respectively, which correspond to the Ga-O bond of the samples, and the binding energy after annealing is reduced by 0.44 eV. The O 1 s peaks were

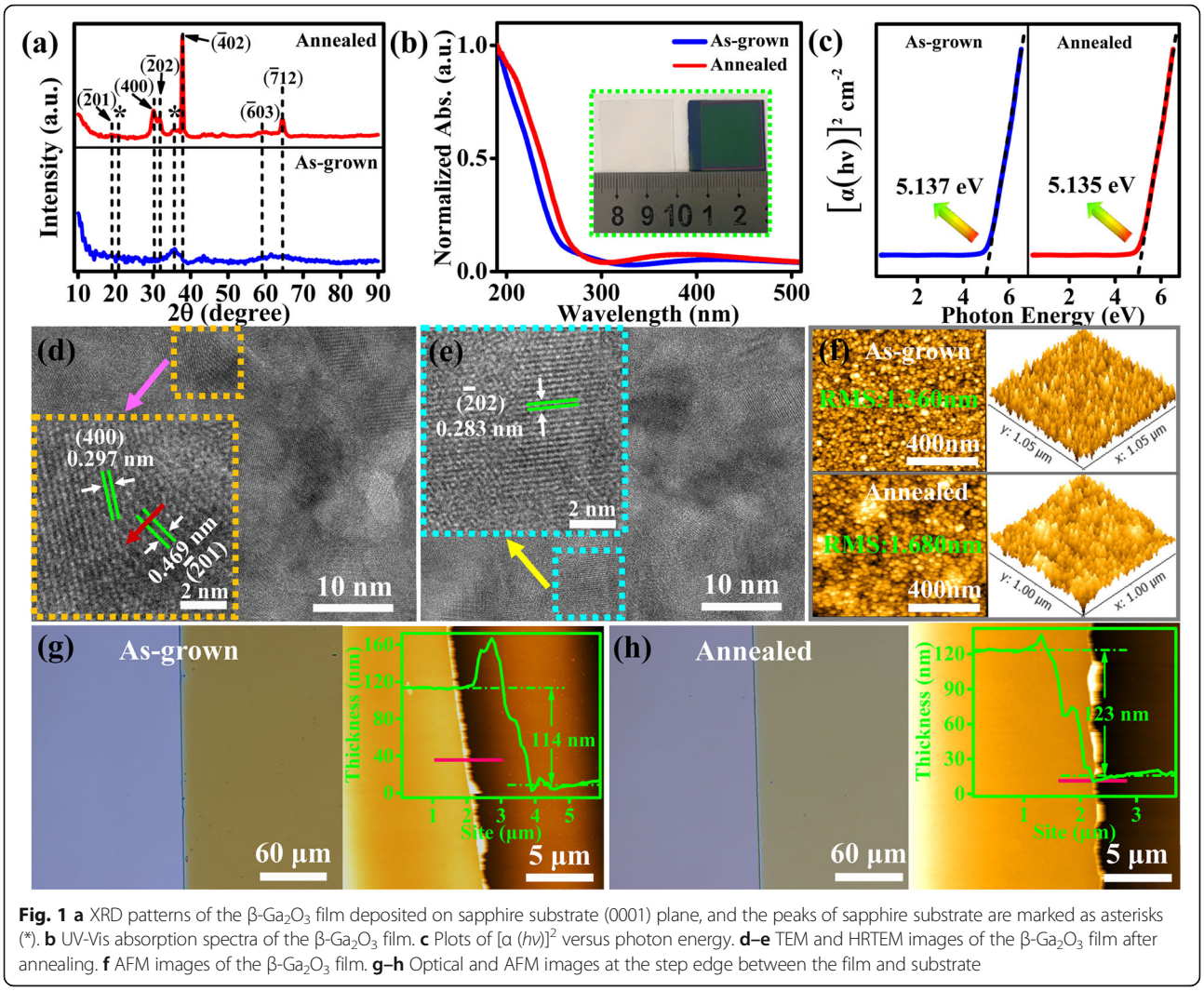


**Fig. 1** **a** XRD patterns of the β-$Ga_2O_3$ film deposited on sapphire substrate (0001) plane, and the peaks of sapphire substrate are marked as asterisks (*). **b** UV-Vis absorption spectra of the β-$Ga_2O_3$ film. **c** Plots of $[\alpha\ (h\nu)]^2$ versus photon energy. **d–e** TEM and HRTEM images of the β-$Ga_2O_3$ film after annealing. **f** AFM images of the β-$Ga_2O_3$ film. **g–h** Optical and AFM images at the step edge between the film and substrate

fitted with two components associated with oxygen vacancies ($O_V$) and lattice oxygen ($O_L$). The area ratios of $O_V$ and $O_L$ (e.g., $S_{OV}$:$S_{OL}$) before and after annealing were 0.47 and 0.12, respectively. This suggests an increase in the lattice oxygen atoms due to the annealing treatment leading to crystallization as oxygen atoms move to their appropriate lattice sites.

An UV photodetector consisting of the β-$Ga_2O_3$ film was fabricated. A simple vertical structure was designed for the photodetector, which comprised of ITO/NiO/$Ga_2O_3$/Al. A schematic diagram of the device structure is shown in Fig. 3a. A NiO layer was first sputtered on an ITO-coated quartz substrate after applying the same wet cleaning procedures as the sapphire substrate, and the detailed preparation and characterizations of NiO film were shown in Additional file 1: Figure S1 and Figure S2. $Ga_2O_3$ layer was then sputtered using the above mentioned deposition parameters. The prepared heterojunction was annealed in air at 600 °C for 30 min to avoid heating damage to ITO (with the knowledge that β-$Ga_2O_3$ can be formed at annealing temperature above 550 °C), followed by vapor deposition of Al electrodes ($2 \times 2\ mm^2$) on the surface of $Ga_2O_3$ film. Finally, the Al electrodes and ITO substrate were used as top and bottom electrodes, respectively.

Figure 3b shows the energy band diagram of the photodetector. We calculated the *Eg* of NiO film according to Eq. (1) as shown in Additional file 1: Figure S3. The *Eg* of NiO film is about 3.4 eV after annealing. The wide bandgap energy of the β-$Ga_2O_3$ (5.1 eV) and NiO (3.4 eV) layers is responsive to UV light. Under UV illumination ($h\nu$), electrons gain enough energy to transit into the conduction band generating electron-hole pairs. These photogenerated electron-hole pairs were separated by the built-in electric field and collected by the respective electrodes. Here, the heterostructure with appropriate band alignment can facilitate the charge separation and collection.

The performance of the heterojunction photodetector was studied from the measured *J-V* and log *J-V* plots,

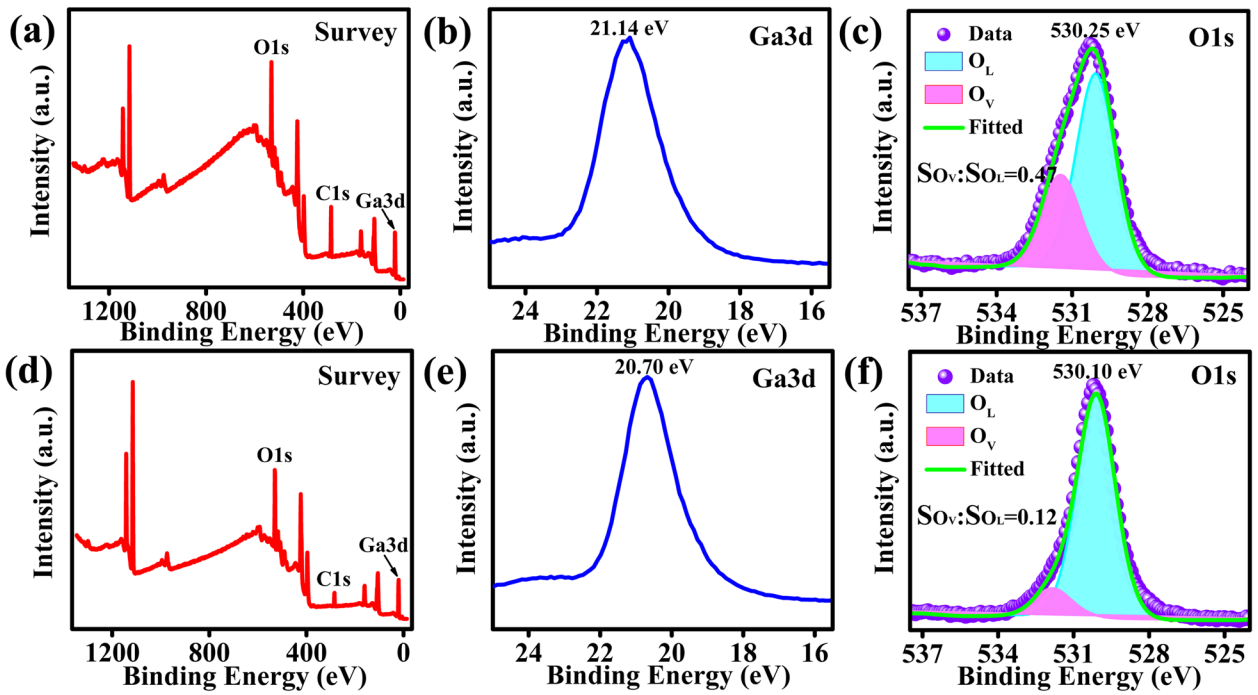


**Fig. 2** XPS spectra of the β-$Ga_2O_3$ film. Survey scan, Ga 3d, and O1s core level peaks acquired before annealing are shown in **a–c** and after annealing are shown in **d–f**, respectively

which were acquired from the backlighting incident device. Figure 3 c and d illustrate the *J-V* and log *J-V* curves of the photodetector illuminated with different wavelength lights and under dark condition, respectively. When the photodetector was illuminated by a 245-nm UV light at 27 μWcm$^{-2}$, a drastic increase of a current density, up to 1.38 mAcm$^{-2}$, was observed at an applied voltage of 10 V. The current density also increases when illuminated with 285 and 365 nm UV lights. However, more electron-hole pairs can be effectively excited by 245 nm UV light compared with other two UV lights, showing the deep UV detection of the device.

*J-V* and log *J-V* curves of the photodetector were measured under an UV illumination of 245 nm with varying power density, as shown in Fig. 3 e and f, respectively. Measurements were performed under dark and UV light conditions. The current density increases with the light intensity under a 245-nm UV illumination which suggests that the photodetector has the ability to generate photocurrent in response to 245 nm UV light.

The effect of bias voltage on the responsivity ($R$) of the device is shown in Fig. 3g. $R$ is related to the photocurrent density ($J_{ph}$) according to Eq. (2) [5]:

$$R = J_{ph}/P_{opt} \tag{2}$$

where $P_{opt}$ is photon power density having a value of 1.5 mWcm$^{-2}$. An increase in $R$ was evident from Fig. 3g as the bias voltage of the device increases under fixed photon power density. The maximum $R$ was 27.43 AW$^{-1}$ measured under a 245-nm illumination (27 μWcm$^{-2}$) at the bias voltage of 10 V.

Detectivity ($D^*$) is another important parameter for evaluating the performance of photodetectors. $D^*$ of the photodetector can be calculated using Eq. (3) as follows [20, 21]:

$$D^* = R/(2q|J_d|)^{1/2} \tag{3}$$

where $q$ is absolute electron charge ($1.602 \times 10^{-19}$ C) and $J_d$ is dark current density. The relationship between $D^*$ and the bias voltage is shown in Fig. 3h, which shows an increase in $D^*$ as the bias voltage increases. The maximum $D^*$ was $3.14 \times 10^{12}$ cmHz$^{1/2}$ W$^{-1}$ measured under a 245-nm illumination (27 μWcm$^{-2}$) at the bias voltage of − 10 V. Based on the values of $R$ and $D^*$, the NiO/β-$Ga_2O_3$ photodetector demonstrated high performance in UV detection, compared with other NiO-based and $Ga_2O_3$-based UV detectors shown in Table 1.

## Conclusions

In conclusion, β-$Ga_2O_3$ film was prepared by RF magnetron sputtering and exhibited good crystallinity after annealing at 800 °C. The wide bandgap material revealed strong UV absorption in the range of 190–300 nm. The deep UV photodetector based on NiO/β-$Ga_2O_3$

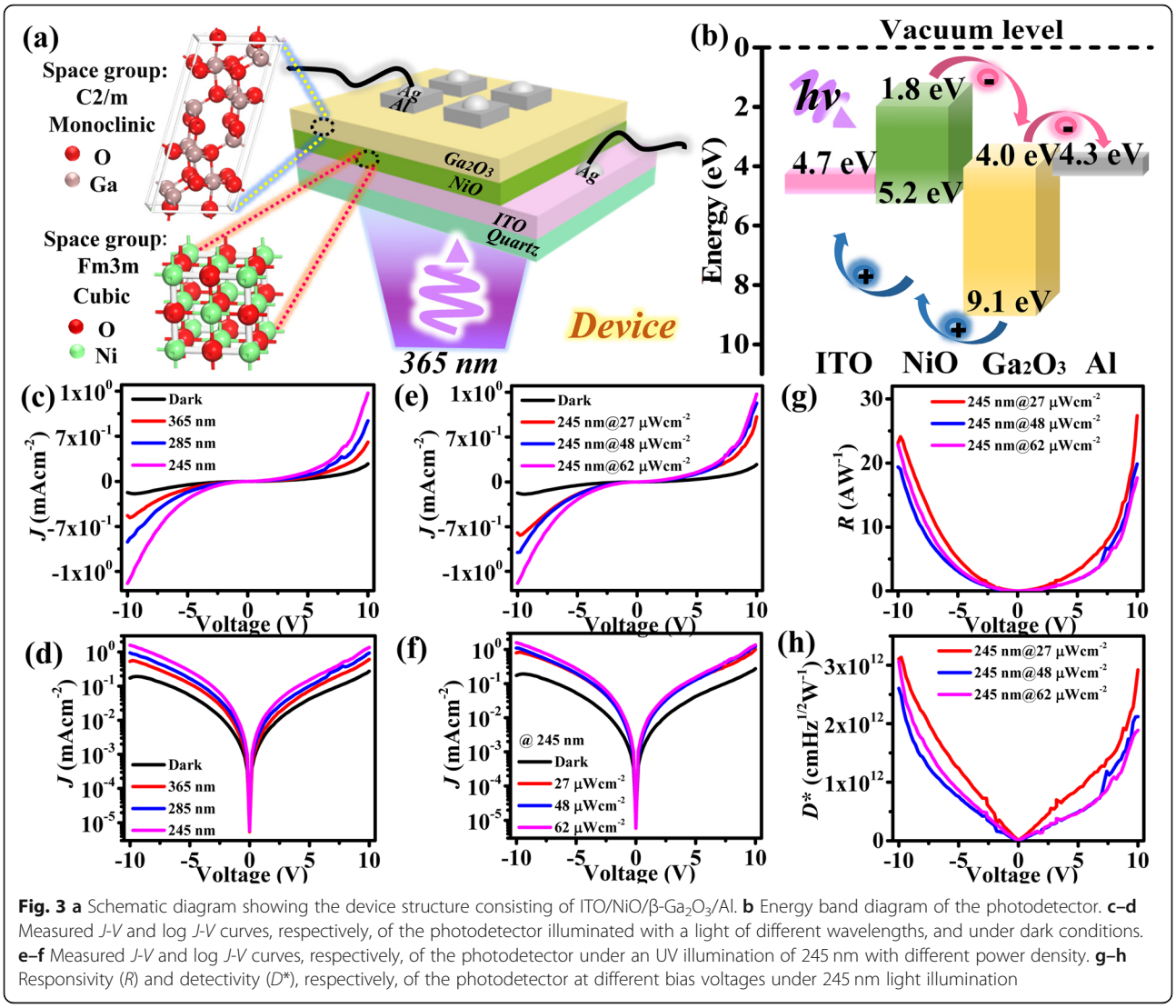


**Fig. 3** **a** Schematic diagram showing the device structure consisting of ITO/NiO/β-$Ga_2O_3$/Al. **b** Energy band diagram of the photodetector. **c–d** Measured *J-V* and log *J-V* curves, respectively, of the photodetector illuminated with a light of different wavelengths, and under dark conditions. **e–f** Measured *J-V* and log *J-V* curves, respectively, of the photodetector under an UV illumination of 245 nm with different power density. **g–h** Responsivity (*R*) and detectivity (*D**), respectively, of the photodetector at different bias voltages under 245 nm light illumination

**Table 1** Comparison of characteristic parameters of other NiO-based and $Ga_2O_3$-based UV detectors

| Device | Preparation method | Wavelength | Bias voltage | *R* ($AW^{-1}$) | Year | Ref. |
|---|---|---|---|---|---|---|
| ITO/NiO/β-$Ga_2O_3$/Al | RF magnetron sputtering | 245 nm | 10 V | 27.43 | – | This work |
| Ni/NiO/ZnO/FTO | RF/DC sputtering | 400 nm | – 5 V | 3.85 | 2015 | [22] |
| Al/ZnO/NiO/ITO | Sol-gel/spin-coating | 350 nm | – 1 V | 10.2 | 2014 | [23] |
| ZnO/$Ga_2O_3$ microwires | CVD | 251 nm | – | $9.7 \times 10^{-3}$ | 2017 | [12] |
| Graphene/β-$Ga_2O_3$ | CVD | – | 20 V | 39.3 | 2016 | [11] |
| GaN/Sn:$Ga_2O_3$ | PLD | 254 nm | – | 3.05 | 2018 | [24] |
| Graphene/β-$Ga_2O_3$ | Mechanical exfoliation | 254 nm | – | 29.8 | 2018 | [25] |
| β-$Ga_2O_3$/Nb:$SrTiO_3$ | RF magnetron sputtering | 254 nm | – 10 V | 43.31 | 2017 | [26] |

heterostructure was highly sensitive to 245 nm UV light with high responsivity ($R$) and detectivity ($D^*$) of up to 27.43 $AW^{-1}$ and $3.14 \times 10^{12}$ $cmHz^{1/2}W^{-1}$, respectively. It is believed that the performances of the UV photodetector can be further improved by means of doping or optimizing the device structure.

## Supplementary information

**Supplementary information** accompanies this paper at https://doi.org/10.1186/s11671-020-3271-9.

**Additional file 1: Figure S1.** XRD patterns of the NiO film deposited on quartz substrate before and after annealing (blue line and red line). **Figure S2.** TEM and HRTEM images of the NiO film after annealing. **Figure S3.** (a) UV-Vis absorption spectra of the NiO film before and after annealing (blue line and red line), the inset is the picture of the prepared film. (b) Plots of $[\alpha (h\nu)]^2$ versus photon energy. **Figure S4.** AFM images of the NiO film after annealing. **Figure S5.** The ohmic contact of Al-$\beta$-$Ga_2O_3$-Al.

### Abbreviations

AFM: Atomic force microscope; ITO: Indium tin oxide; TEM: Transmission electron microscope; UV: Ultraviolet; XPS: X-ray photoelectron spectroscopy; XRD: X-ray diffraction

### Acknowledgements

This work was supported by the National Natural Science Foundation of China (grant nos. 61106098, 51462037, and 11864044), the Key Project of Applied Basic Research of Yunnan Province, China (grant no. 2012FA003), PolyU grants (1-ZVGH and 1-BBAD), and Research Grants Council of Hong Kong (project nos.: PolyU153030/15P, PolyU153271/16P, and PolyU 153039/17P).

### Authors' Contributions

MJ carried out the experiments and drafted the manuscript. LT designed the experiments. LT and JX supervised the experiments. FW, KST, and SPL participated in the discussion and analyzing of the experimental results. LT, JX, KST, and SPL helped to draft and revise the manuscript. All authors read and approved the final manuscript.

### Availability of Data and Materials

The conclusions made in this manuscript are based on the data (main text and figures) presented and shown in this paper.

### Competing Interests

The authors declare that they have no competing interests.

### Author details

[1]School of Materials Science and Engineering, Yunnan University, Kunming 650091, China. [2]Kunming Institute of Physics, Kunming 650223, China. [3]Yunnan Key Laboratory of Advanced Photoelectric Materials & Devices, Kunming 650223, China. [4]School of Physics and Astronomy, Yunnan University, Kunming 650091, China. [5]College of Engineering, Swansea University, Bay Campus, Fabian Way, Swansea SA1 8EN, UK. [6]Department of Applied Physics, The Hong Kong Polytechnic University, Hung Hom, Kowloon, Hong Kong, China.

Received: 5 December 2019 Accepted: 28 January 2020
Published online: 22 February 2020

### References

1. Wang X, Tian W, Liao M, Bando Y, Golberg D (2014) Recent advances in solution-processed inorganic nanofilm photodetectors. Chem Soc Rev 43:1400–1422
2. Kim M, Seo JH, Singisetti U, Ma Z (2017) Recent advances in free-standing single crystalline wide band-gap semiconductors and their applications: GaN, SiC, ZnO, β-$Ga_2O_3$, and diamond. J Mater Chem C 5:8338
3. Chang H, Lee DH, Kim HS, Park J, Lee BY (2018) Facile fabrication of self-assembled ZnO nanowire network channels and its gate-controlled UV detection. Nanoscale Res Lett 13:413
4. Sun X, Azad F, Wang S, Zhao L, Su S (2018) Low-cost flexible ZnO microwires array ultraviolet photodetector embedded in PAVL substrate. Nanoscale Res. Lett 13:277
5. Liu X, Gu L, Zhang Q, Wu J, Long Y, Fan Z (2014) All-printable band-edge modulated ZnO nanowire photodetectors with ultra-high detectivity. Nat Commun 5:4007
6. Xie Y, Wei L, Wei G, Li Q, Jiao J (2013) A self-powered UV photodetector based on $TiO_2$ nanorod arrays. Nanoscale Res Lett 8:188
7. Li X, Gao C, Duan H, Lu B, Pan X, Xie E (2012) Nanocrystalline $TiO_2$ film based photoelectrochemical cell as self-powered UV-photodetector. Nano Energy 1:640–645
8. Wei T, Chao Z, Tianyou Z, Song-Lin L, Xi W, Meiyong L, Kazuhito T, Dmitri G, Yoshio B (2013) Flexible $SnO_2$ hollow nanosphere film based high-performance ultraviolet photodetector. Chem Commun 49:3739–3741
9. Zhang Y, Tao J, Zhang W, Guan G, Ren Q, Xu K, Huang X, Zou R, Hu J (2017) A self-powered broadband photodetector based on n-Si (111)/p-NiO heterojunction with high photosensitivity and enhanced external quantum efficiency. J Mater Chem C 5:12520–12528
10. Zou R, Zhang Z, Liu Q, Hu J, Sang L, Liao M, Zhang W (2014) High detectivity solar-blind high-temperature deep-ultraviolet photodetector based on multi-layered (l00) facet-oriented β-$Ga_2O_3$ nanobelts. Small 10:1848–1856
11. Kong WY, Wu GA, Wang KY, Zhang TF, Zou YF, Wang DD, Luo LB (2016) Graphene-β-$Ga_2O_3$ heterojunction for highly sensitive deep UV photodetector application. Adv Mater 28:10725
12. Zhao B, Fei W, Chen H, Zheng L, Su L, Zhao D, Fang X (2017) An ultrahigh responsivity (9.7 $mAW^{-1}$) self-powered solar-blind photodetector based on individual ZnO-$Ga_2O_3$ heterostructures. Adv. Funct. Mater 27:1700264
13. Zhao B, Wang F, Chen H, Wang Y, Jiang M, Fang X, Zhao D (2015) Solar-blind avalanche photodetector based on single ZnO-$Ga_2O_3$ core-shell microwire. Nano Lett 15:3988
14. Kokubun Y, Kubo S, Nakagomi S (2016) All-oxide p–n heterojunction diodes comprising p-type NiO and n-type β-$Ga_2O_3$. Appl Phys Express 9:091101
15. Kokubun Y, Miura K, Endo F, Nakagomi S (2007) Sol-gel prepared β-$Ga_2O_3$ thin films for ultraviolet photodetectors. Appl Phys Lett 90:031912
16. Guo XC, Hao NH, Guo DY, Wu ZP, An YH, Chu XL, Li LH, Li PG, Lei M, Tang WH (2016) β-$Ga_2O_3$/p-Si heterojunction solar-blind ultraviolet photodetector with enhanced photoelectric responsivity. J Alloys Compd 660:136–140
17. Li Y, Tokizono T, Liao M, Miao Z, Koide Y, Yamada I, Delaunay JJ (2010) Efficient assembly of bridged β-$Ga_2O_3$ nanowires for solar-blind photodetection. Adv Funct Mater 20:3972–3978
18. Hwang JD, Chen HY, Chen YH (2018) Effect of nickel diffusion and oxygen behavior on heterojunction Schottky diodes of Au/NiO/ZnO with a NiO interlayer prepared by radio-frequency magnetron sputtering. Nanotechnol. 29:295705
19. Hao SJ, Hetzl M, Schuster F, Danielewicz K, Bergmaier A, Dollinger G, Sai QL, Xia CT, Hoffmann T, Wiesinger M, Matich S, Aigner W, Stutzmann M (2019) Growth and characterization of β-$Ga_2O_3$ thin films on different substrates. J Appl Phys 125:105701
20. Yang Y, Dai H, Yang F, Zhang Y, Luo D, Zhang X, Wang K, Sun XW, Yao J (2019) All-perovskite photodetector with fast response. Nanoscale Res Lett 14:291
21. Gong X, Tong M, Xia Y, Cai W, Moon JS, Cao Y, Yu G, Shieh CL, Nilsson B, Heeger AJ (2009) High-detectivity polymer photodetectors with spectral response from 300 nm to 1450 nm. Science 325:1665–1667
22. Patel M, Kim H-S, Kim J (2015) All transparent metal oxide ultraviolet photodetector. Adv Electron Mater 1:1500232
23. Kim DY, Ryu J, Manders J, Lee J, So F (2014) Air-stable, solution-processed oxide p-n heterojunction ultraviolet photodetector. ACS Appl Mater Interfaces 6:1370–1374
24. Guo D, Su Y, Shi H, Li P, Zhao N, Ye J, Wang S, Liu A, Chen Z, Li C, Tang W (2018) Self-powered ultraviolet photodetector with superhigh photoresponsivity (3.05 A/W) based on the GaN/Sn: $Ga_2O_3$ pn junction. ACS Nano 12:12827–12835
25. Oh S, Kim C-K, Kim J (2018) High responsivity β-$Ga_2O_3$ metal-semiconductor-metal solar-blind photodetectors with ultraviolet transparent graphene electrodes. ACS Photonics 5:1123–1128
26. Guo D, Liu H, Li P, Wu Z, Wang S, Cui C, Li C, Tang W (2017) Zero-power-consumption solar-blind photodetector based on beta-$Ga_2O_3$/NSTO heterojunction. ACS Appl Mater Interfaces 9:1619–1628

## Publisher's Note